Brief Review

Modern Physics Letters B, Vol. 19, No. 26 (2005) 1303–1322

World Scientific
www.worldscientific.com

QUARTZ CRYSTAL RESONATOR BASED SCANNING PROBE MICROSCOPY

YONGHO SEO* and SEUNGBUM HONG

Samsung Advanced Institute of Technology,
Mt. 14-1, Nongseo-Ri, Giheung-Eup, Yongin-Si, Gyeonggi-Do, 449-712 South Korea
**yongho1.seo@samsung.com*

Received 15 September 2005

The piezoelectric quartz crystal resonator is a common electronic device used for a reference clock which has high Q-valued resonance. In this paper, a general description on the quartz crystal resonator based scanning probe microscopy is presented. Most well-known type of the quartz crystal resonator is the tuning fork which has been employed as a force sensor in many different types of the scanning probe microscopy. The most important advantage of the quartz crystal resonator based scanning probe microscopy is high resolution imaging. Furthermore, it has potential to be used at low temperature due to its low power dissipation, compactness, and non-optical detection.

Keywords: Scanning probe microscopy; quartz crystal resonator; atomic force microscopy; tuning fork.

1. Introduction

Since the scanning tunnelling microscope (STM) was first invented by Binnig *et al.*,[1] scanning probe microscopy (SPM) has been a most important tool to explore the nano-scale nature. The SPM has been developed with variety of different types for different experimental purposes, including STM, atomic force microscopy (AFM),[2] near-field scanning optical microscopy (NSOM),[3] magnetic force microscopy (MFM),[4,5] electrostatic force microscopy (EFM),[6] etc. Most of those microscopes except STM are based on the micro-fabricated cantilever and optical deflection technique to control the distance. Even though the optical deflection technique allows good performances, it has critical disadvantages for some specific applications. For example, for *in situ* measurement in a vacuum chamber, cryogenic environment measurement, or dark environment measurement, the optical deflection technique cannot be employed. This is a reason why one cannot built an ultra high vacuum (UHV) STM combined with a cantilever based AFM. Specifically, there are many weak points of the optical deflection technique; (i) taking large space, (ii) inconvenience of optical alignment, (iii) vulnerability to external noise, (iv) unavoidable optical exposure, and (v) high dissipative power.

One alternative method of optical detection is fiber optic interferometry.[7,8] Typically, the fiber optics interferometry has been employed for high vacuum or cryogenic instruments. All the optical source and detection electronics are installed outside the vacuum chamber. Through an optical fiber, the optics are connected to the microscope head. The end of the optical fiber is cleaved and located close to the top of the cantilever. The interferometric signal between the cantilever and fiber cleaved surface is used for distance measurement. Typically, this approach is used for many low temperature SPMs. However, one of disadvantages of the fiber-optic interferometry is that the design of the microscope is too complicated to be used for a dilution refrigerator. It requires more than two coarse approach mechanisms in order to align the optical fiber, cantilever, and sample. To reduce the complexity of the SPM design, non-optical (all-electric) detection methods have been developed.

As a representative example of the electric detection methods, piezoresistive cantilever detection has been widely studied.[9,10] While piezoresistive cantilever detection has advantages such as simple design and electrical detection without optics, it has serious drawbacks such as low signal-to-noise ratio and excessive heat dissipation.

Another way for electric detection is using quartz crystal resonator (QCR)[11] as a force sensor. The QCR based SPM has many advantages overcoming the drawbacks of the other type SPMs.

(1) As the tuning fork is a self-dithering and self-sensing device, no optics are required and the head can be very simple and compact.
(2) Because the QCR sensor is stiff and the dithering amplitude is small, it allows high resolution SPM.
(3) Because no light source is necessary and the dissipated power can be reduced down to $\sim$ 1 pW,[12] QCR based SPM can be operated in the dark and low temperature conditions.
(4) As the QCR is common and cheap device, one can manufacture the SPM at a low cost.

Recently, a micro-machined quartz crystal cantilever has reported by Ono, *et al.*[13] With the conventional micro-fabrication process on the quartz crystal wafer instead of Si wafer, the *quartz cantilever* was invented. Without any optical component, it operates electrically, with electrodes on the quartz cantilever. They opened the door to replace all the Si based cantilever into the quartz crystal based cantilever.

There are many different types of the QCRs having different shapes, vibrational modes and directions. The most well-known type in SPM field is the tuning fork as shown in Fig. 1(a). The tuning fork has two prongs vibrating in the opposite direction with flexural mode. Typically, it has 32768 Hz resonance frequency. Its commercial usage is for wrist watches. A trident QCR as shown in Fig. 1(b) has three prongs vibrating in extensional mode. The trident QCR has 1 MHz resonance frequency. Another type of QCR so-called needle sensor[14,15] is shown in Fig. 1(c) of

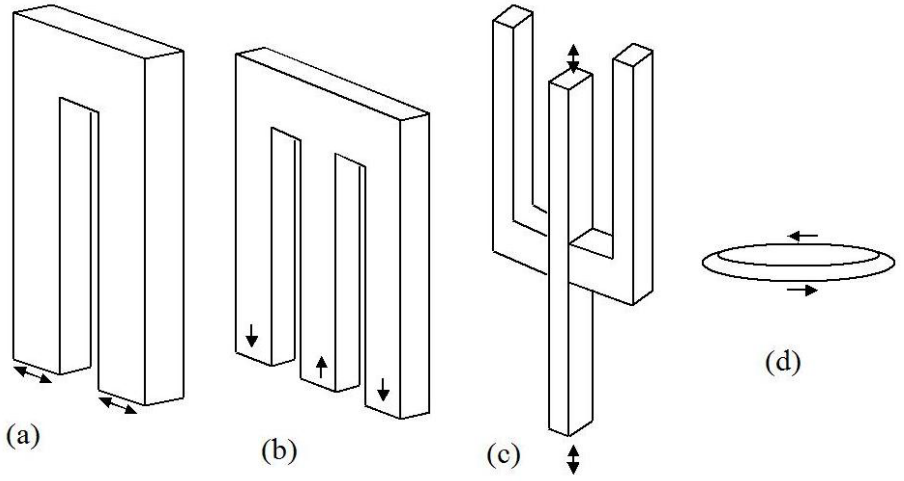

Fig. 1. There are many different types of quartz crystal resonator; (a) a tuning fork, (b) trident QCR, (c) needle sensor, and (d) AT-cut QCR.

which physical properties are similar to the trident QCR. The most common type of QCR is AT-cut high frequency QCR as shown in Fig. 1(d). Its frequency range covers from 2 to 100 MHz and it has thickness shear vibration mode.

2. Principle

2.1. *Driven oscillator model*

A vibrational motion of the QCR can be considered as a driven damped oscillator.[16] Two (or three) ends of QCR prongs correspond to antinodes and a node is located in the middle of two antinodes. To make the problem simple, we can consider the motion of a prong as a fixed-end (node) and free-end (antinode) string model. Therefore, the motion of a prong can be considered as a 1-dimensional driven oscillator. In case of the tuning fork, a flexural motion spring constant of a prong is obtained from the formula $k = Ewt^3/(4l^3)$, where $E = 7.87 \times 10^{10}$ N/m^2 is the Young modulus of the quartz, where w is the width, t thickness, and l length.[17,18] In case of extensional motion such as trident QCR and needle sensor, $k = AE/l$, where A is the cross sectional area ($A = wt$).[19] When a sinusoidal force $F_0 \cos \omega t$ is applied to the resonator, the equation of motion is given as

$$m_e \ddot{z} + 2b\dot{z} + kz = F_0 \cos \omega t \,, \tag{1}$$

where z is the displacement of the resonator, b is damping constant, $m_e = m/4$ is effective mass of a prong.[18] A steady state particular solution is given as[16]

$$z(t) = \frac{A}{\sqrt{(\omega_0^2 - \omega^2)^2 + 4\omega^2\beta^2}} \cos(\omega t - \delta) \tag{2}$$

with

$$\delta = \tan^{-1} \frac{2\omega\beta}{\omega_0^2 - \omega^2}\,, \tag{3}$$

where $\beta = b/m_e$ and $\omega_0 = \sqrt{k/m_e}$ is the resonance frequency. The quantity δ represents the phase difference between the driving force and the resultant motion. It is noticeable that the phase difference is $\pi/2$ at $\omega = \omega_0$. It is customary to describe the degree of damping in an oscillating system in terms of the quality factor or the Q of the system:

$$Q = \frac{\sqrt{\omega_0^2 - 2(b/m_e)^2}}{2b/m_e} \simeq \frac{\omega_0}{\Delta\omega}\,, \tag{4}$$

where $\Delta\omega$ represents the frequency interval between the points on the amplitude resonance curve that is 0.707 of the maximum amplitude.

There is another solution which has envelop of $e^{-b/m_e t}$ due to transient effect. This effect will be disappeared, eventually and is not important in long time scale. However, in SPM experiments, the oscillator continuously scans a sample and immediate feedback should be given, so the transient effect is critical issue for scanning speed. The time scale of transient effect is

$$\tau \simeq m_e/b \simeq 2Q/\omega_0\,. \tag{5}$$

As a result, a high Q-value causes a slower response. For a tuning fork with $Q = 10^4$, typically, $\tau \simeq 200$ ms, which is unacceptably slow for most applications.

2.2. *Sensitivity and thermal noise*

For a one-dimensional harmonic oscillator, the thermal vibrational motion is given by $\delta z^2 = k_B T/k$ on resonance over a self-limited bandwidth of $1/\tau$ from the equipartition theorem.[20] At temperature $T = 300$ K, this thermal noise amounts to $\langle \delta z^2 \rangle^{1/2} \sim 1$ pm, with k in order of 10^4 N/m. Typically, the thermal noise measurement provides a good indication of the detection performance.

When a uniform force is applied on a harmonic oscillator, its resonance frequency is not changed. If a non-uniform force is applied, its frequency will be changed. Simply, we can find the relation between the force gradient $\partial F/\partial z$ and frequency shift Δf, from the equation of motion

$$F' = F + \frac{\partial F}{\partial z} z = k' z\,, \tag{6}$$

where F' and k' are the modified force and spring constant, respectively. Then the modified angular frequency

$$\omega' = \sqrt{\frac{k}{m} + \frac{1}{m}\frac{\partial F}{\partial z}}\,. \tag{7}$$

As a result, the frequency shift is

$$\Delta f \simeq \frac{1}{2}\frac{f}{k}\frac{\partial F}{\partial z}\,. \tag{8}$$

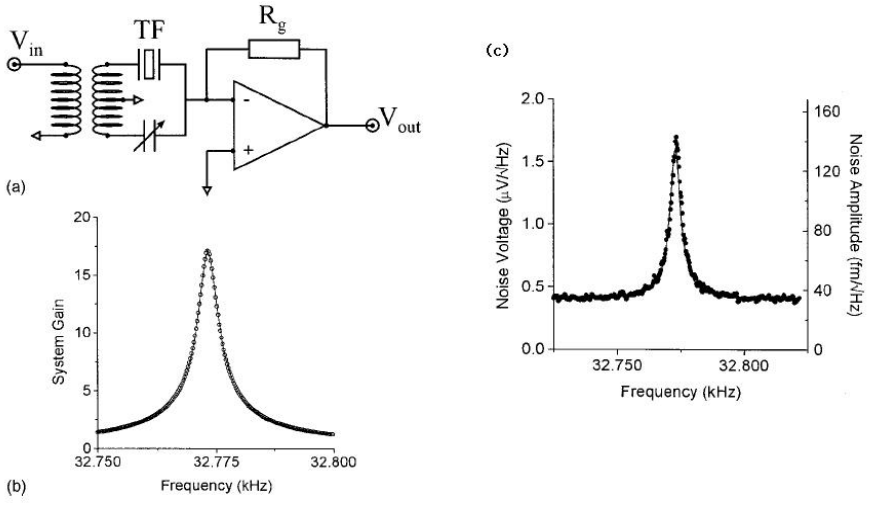

Fig. 2. (a) The current to voltage amplifier circuit diagram for a tuning fork suggested by Grober *et al.* A transformer and variable capacitor are to eliminate the effect of the static capacitor. (b) The output signal spectrum when an ac voltage was applied to the circuit input. (c) The noise spectrum of the circuit. No input signal was applied. The solid line is a fitting result. (From Grober *et al.* (2000).)

From Eq. (8), one can figure out the relation between the force gradient and frequency shift. In order to have good force sensitivity, high frequency and low stiffness are favorable.

Grober *et al.*[21] suggested a theoretical model for the sensitivity of the tuning fork. An operational amplifier circuit was used to convert the net current to a voltage as shown in Fig. 2(a). The current to voltage (V_{out}/I) gain shows RC-damping behavior as a function of frequency f: $Z_{\text{gain}} = R_g/\sqrt{1+(2\pi f R_g C_g)^2}$, where R_g, and C_g are resistance of the load resistor and a stray capacitance in parallel with R_g. An AC voltage (V_{in}) was applied to the tuning fork and the output voltage (V_{out}) was fit to the Lorentzian line shape

$$V_{\text{out}}/V_{\text{in}} = \frac{Af_0 f/Q}{\sqrt{(f_0^2 - f^2)^2 + (f_0 f/Q)^2}}\,, \tag{9}$$

where A, f_0, and Q are fitting parameters. The fitting result is as shown in Fig. 2(b). This wave form is exactly the same as RLC resonator. By comparing the line shape, the equivalent RLC circuit parameters can be calculated, where $R = Z_{\text{gain}}/A$.

On this system, there are two primary noise sources: Johnson noise of the feedback resistor($\sqrt{4k_BTR_g}$) and Johnson noise associated with mechanical dissipation in the fork ($\sqrt{4k_BTR}\cdot V_{\text{out}}/V_{\text{in}}$). These two noise terms add in quadrature and that was fitted into the measured data as shown in Fig. 2(c). The power spectrum of the noise associated with the tuning fork can be integrated so as to obtain the root mean square voltage noise.

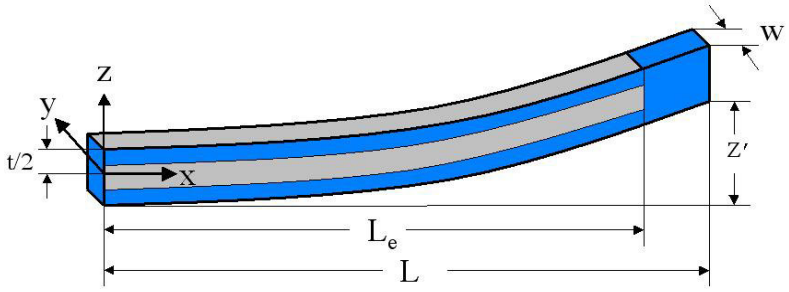

Fig. 3. A prong of a tuning fork which has two electrodes at both sides.

$$V_{\text{rms}}^2 = \int_0^\infty 4k_BTR\frac{(Af_0f/Q)^2}{(f_0^2-f^2)^2+(f_0f/Q)^2}df = 4k_BTR\left(\frac{Z_{\text{gain}}}{R}\right)^2\left(\frac{\pi f_0}{2Q}\right). \quad (10)$$

Particularly, $V_{\text{rms}} = 3.81\ \mu\text{V}$ on their system.

Giessibl[20] suggested a theoretical model to calculate the sensitivity of the tuning fork. When a force $F = kz'$ is acting on a prong of the tuning fork (Fig. 3), the strain ϵ at the upper side electrode (contracted) is given by

$$\epsilon(x, z = t/2) = \frac{t}{2}kz' \cdot (x - L)\frac{1}{EJ}, \quad (11)$$

where E is Young's modulus and J is the moment of inertia $J = wt^3/12$.[17] This strain causes a surface charge density $\sigma_{\text{charge}} = d_{21}\epsilon E$ where d_{21} is the piezoelectric coupling constant ($d_{21} = 2.31\times10^{-12}$ C/N for quartz). The charge q_{top} accumulated on the top electrode is obtained by integrating the surface charge density as below

$$q_{\text{top}} = \int_0^w \int_0^{L_e} \sigma_{\text{charge}}dxdy = 6z'd_{21}kL_e(L_e/2 - L)/t^2. \quad (12)$$

The same amount of the charge is accumulated on the bottom electrode (inflated, not shown on the figure). The total charge $q = 2q_{\text{top}}$. If the applied force is vibrating with the resonance frequency, $z' = A\cos(2\pi f\tau)$, where A is the vibration amplitude. The induced voltage V can be calculated from $V = IR = R \cdot dq/d\tau$, where R is the load resistor of the current to voltage amplifier. Finally, the sensitivity defined as $S = V/A$ is

$$S = 24\pi fRd_{21}kL_e(L - L_e/2)/t^2\,. \quad (13)$$

Particularly on his experiment, $L \simeq 2.4$ mm, $L_e \simeq 1.6$ mm, $t \simeq 0.21$ mm, $k \simeq 1800$ N/m, $f = 25.8$ kHz, and $R = 100$ MΩ. As a result, the sensitivity $S \simeq 45\ \mu$V/pm.

2.3. *PLL detection scheme*

Since Guethner *et al.* employed a tuning fork for AFM, the tuning fork based SPM has been developed in almost all kinds of the SPM family including AFM, NSOM, MFM, EFM etc.[12,18,20,22,24,39]

In spite of many advantages, two critical drawbacks of the tuning fork caused delay in its practical use; high stiffness and slow response. The former can be compensated by increasing its quality factor. The later might be more serious problem in high quality factor resonator as calculated at Eq. (5). Especially, at low temperature, the QCRs have exceptionally high quality factor and its response is unacceptably slow. In order to overcome this problem, phase-locked-loop (PLL) detection schemes were suggested.[12,23,24]

According to Atia and Davis's argument, if the force detection mechanism is not purely dissipative, but also includes a conservative component that changes the effective compliance of the resonator, then its resonance frequency will change instantaneously independent of the quality factor.[23] Because of that, the frequency control mechanism was required.

The PLL consists of two parts: voltage controlled oscillator (VCO) and phase detector. From the VCO, an ac reference signal is generated. The reference signal is fed to a resonator. The resonator induces a response signal. The phase detector measures the phase difference between the response signal and the reference signal. The phase detector generates an error signal proportional to the phase difference. The error signal gives a feedback to the VCO. Finally, the VCO adjusts the frequency of the reference signal to match the phase difference to be a $\pi/2$. In this way, the reference signal frequency will be always the same as the resonance frequency of the resonator.

As shown in Fig. 4(a), Atia and Davis used a reference input signal which has a fixed frequency. With a positive feedback oscillation circuit, the tuning fork oscillates with its own resonance frequency. A phase detector generates an error signal proportional to the phase difference between the reference input signal and the tuning fork resonance signal. The error signal gives a feedback to the piezo actuator z-directional motion for the resonance frequency to be equal to the reference signal frequency.

On the other hand, Edwards *et al.* suggested a different version of a PLL scheme, the external VCO was employed to control the frequency of the reference signal as shown in Fig. 4(b). The VCO consists of a digital signal processor and a digital frequency synthesizer. This system has its unique feature with voltage divider and preamplifier mounted closely on the AFM body.

As the PLL detection scheme became established, a commercial version of the PLL (EasyPLL, Nanosurf) having frequency resolution in order of mHz was developed and its usage has explosively increased in the tuning fork based SPM society.

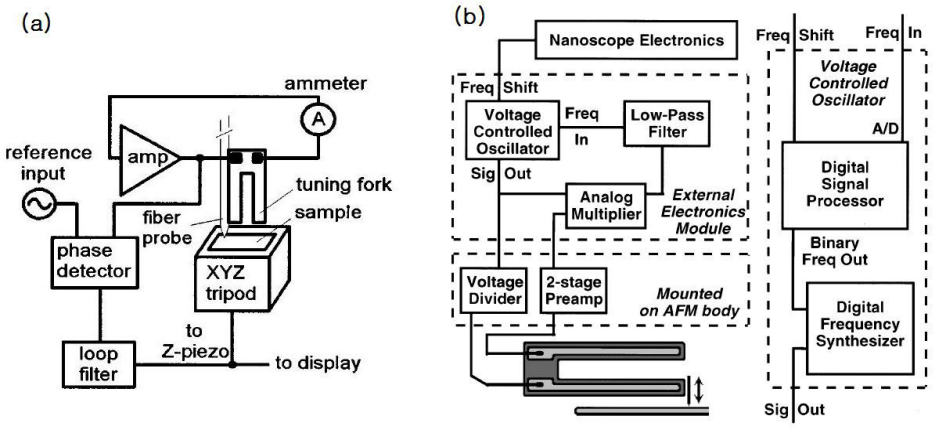

Fig. 4. (a) Schematic diagrams of phase detection scheme suggested by Atia and Davis. The tuning fork itself serves as a voltage controlled oscillator. (From Atia and Davis.) (b) A PLL design suggested by Edwards *et al.* The customized voltage controlled oscillator using digital signal processor was developed. (From Edwards *et al.* (1997).)

3. Quartz Crystal Resonator Based NSOM

3.1. *Tuning fork based NSOM*

While apertureless NSOM uses a metal coated cantilever as a probe, aperture NSOM cannot use a micro fabricated cantilever, because an optical fiber is too bulky to be mounted on the cantilever. In the earlier, the optical fiber was vibrated by an actuator such as bimorph and its motion was measured by optical detection. Optical detection of the tip vibration amplitude can be performed by differential interferometry or by measuring the intensity of reflected laser beam focused on the optical fiber end. Although such methods are proven to allow reliable operation in friendly experimental conditions, they are not convenient for operation at low temperatures, in high vacuum conditions, or in situations space is restricted. In an effort to avoid those problems, Karrai and Grober employed the tuning fork for aperture NSOM, first.[18]

Figure 5(a) shows a crystal quartz tuning fork with an optical fiber tip glued along one of its prongs. The tuning fork was vibrated along X-axis (shear mode). The gray areas indicate electrodes for the piezoelectric signal. An ac voltage was applied to the electrode A, and the induced current at the electrode B was converted into a voltage. Figure 5(b) shows amplitude of the piezoelectric signal as a function of the driving frequency. These experimental data were fitted onto the driven damped oscillator model (solid line). The inset shows thermal noise spectrum, for the tuning fork at 300 K with no driving voltage on the electrode. As the tuning fork tip approaches a surface, the amplitude change was detected. Using this amplitude change, the distance was controlled and a topographic image was obtained, successfully.

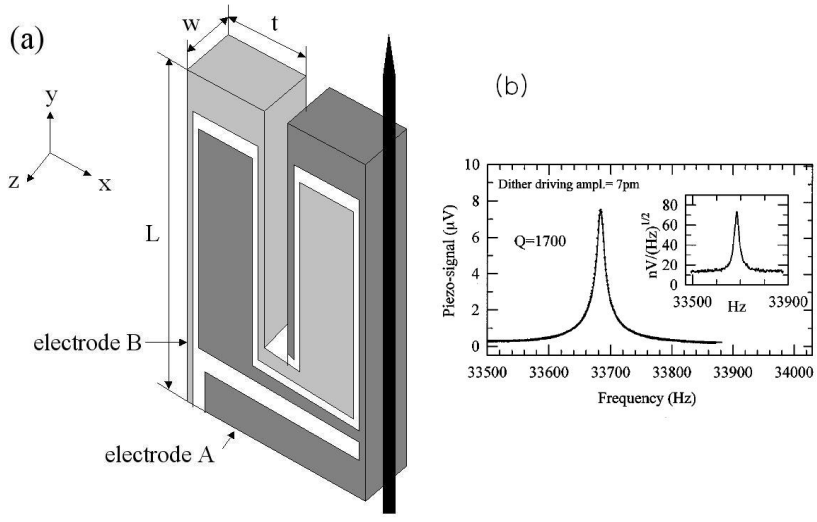

Fig. 5. (a) A quartz crystal tuning fork with tapered optical fiber tip glued on one prong. (b) Amplitude of the piezoelectric signal as function of the driving frequency. The inset shows noise signal, for the freely oscillating fork. (From Karrai and Grober (1995).)

3.2. *Variations of NSOM using QCRs*

Tsai and Lu suggested a tapping mode NSOM using a tuning fork.[25] They attached an optical fiber normal to the longitudinal direction of a tuning fork prong as shown in Fig. 6(a). The other prong was attached on a piezoelectric bimorph, which vibrated the tuning fork. For the tapping mode, the tip vibrates in vertical direction on the sample. The higher spatial resolution is expected than the shear mode, because the tip touches one point not sweeping the sample, in tapping mode.

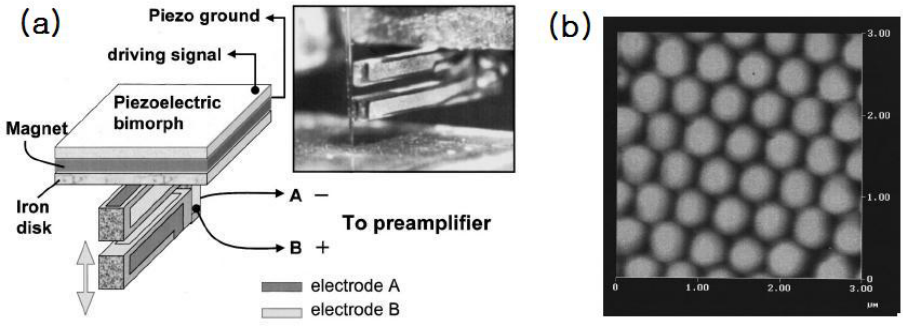

Fig. 6. (a) Illustration and photograph of the tapping mode NSOM demonstrated by Tsai and Lu. (b) A topographic AFM image obtained by using the tapping mode NSOM. (From Tsai and Lu (1998).)

Figure 6(b) shows a tapping-mode 3 μm $\times$ 3 μm AFM image of a close-packed layer of polystyrene spheres in air.

Seo *et al*, demonstrated a high-speed AFM and NSOM using a fiber tip attached to an AT-cut QCR vibrating at 2.0 MHz resonance frequency.[26,27] With a high-frequency dithering probe, they obtained images at the scanning speed of 1.2 mm/s and it took only 0.5 s to image the surface area of 55 μm^2 for 64×64 pixels. It is natural that high frequency QCR allows its fast scanning. However, its drawback is its high stiffness. In an effort to integrate the QCR on a chip, the micro-fabricated high frequency QCR is being developed, which is expected to be a promising candidate for a next-generation SPM sensor.

Instead of the NSOM using an optical fiber, Wilde *et al.* presented a design of an apertureless NSOM using a metallic tip.[28] The system operated in tapping mode with an electrochemically etched tungsten tip mounted on a quartz tuning fork. The tip scattered the near field at the sample surface. They used a tuning fork with $k = 8500$ N/m. They obtained topographical and optical images of subwavelength holes in a chromium film, successfully. The light sources were in the visible ($\lambda = 655$ nm) and the infrared ($\lambda = 10.6$ μm) ranges. A few tens nm resolution was achieved.

Kim *et al.* demonstrated a scanning near-field microwave microscope (NSMM) in the liquid environment by using a tuning fork ($k = 8700$ N/m, $Q = 500$) shear force detection.[29] As the tip immersed in water, the Q-value dropped below 300. The tip attached to one prong of the tuning fork was coupled to a high-quality dielectric resonator ($f = 4.5 \sim 5.5$ GHz). The amplitude of the tuning fork was controlled to keep the distance between the tip and sample. They obtained the topographic and NSMM images of a DNA sample in air and liquid, successfully.

On the other hand, the topographic imaging in liquid was studied by Hulst group, also.[30,31] They presented a study of the dynamic behavior of tuning forks and the application of tuning fork based SPM on soft samples in liquid. Its resonance frequency and vibration amplitude shifts were observed upon immersion into liquid. Due to high Q-value, upon complete immersion into liquid, they obtained high-resolution images on soft samples in liquid. Their study opened a door for biological applications with tuning fork based NSOM.

4. High Resolution AFM

4.1. *q-plus sensor*

If a tip was attached to a prong, the symmetry of the prongs is broken, when one of them is subject to a tip sample interaction. The other prong having high quality factor causes slow scanning speed. Furthermore, it is very difficult to interpret its coupled signal. Giessibl suggested a design *qPlus-sensor*[12] attaching one of the prongs firmly to a supporting structure as shown in Fig. 7(a). His design allows using tuning forks in a similar manner as conventional cantilevers in AFM. The qPlus-sensor has additional advantages. It has mechanical stability, which is essential

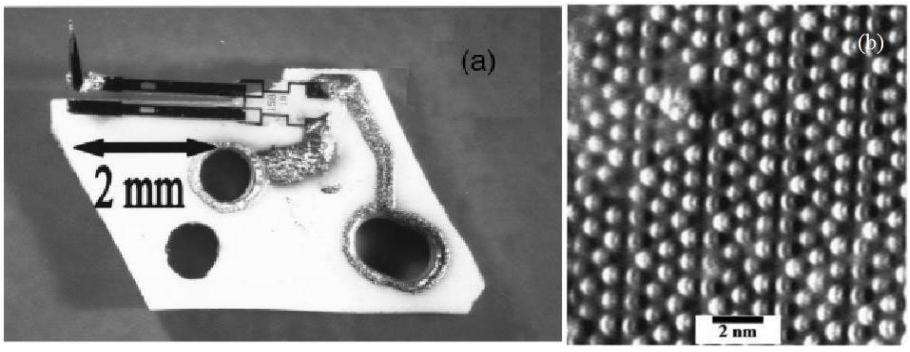

Fig. 7. (a) Photograph of the tuning fork sensor with qPlus configuration. One of the prongs of a quartz tuning fork is attached to a substrate, a tungsten tip is mounted to the other prong. (b) Non-contact topographic AFM image of Si(111)-(7×7) imaged by Giessibl. (From Giessible (2000).)

factor determining the resistance of floor vibration or sound noise. It is easy to interpret the signal, because the signal comes only from the sample-tip interaction. A slow response come from a prong which has no tip is eliminated. One technical challenge is improving the quality factor of it. Typically, when a prong of the tuning fork is attached on a supporting structure, its Q-value decreases unacceptably. To keep the high Q-value, the glue should be very strong. To date, the suitable attaching method with robustness and reliability has not been established.

4.2. *Atomic resolution AFM*

Since it was imaged with STM by Binnig *et al.*,[1] the Si 7×7 structure imaging became a typical experiment showing a true atomic resolution capability. In case of contact mode AFM, it sometimes shows atomic corrugation. But the regular pattern of atomic scale should be distinguished from the true atomic resolution, because the regular pattern can be made not by a single atom, but by a collective interaction of atoms. The critical parameter determining the true atomic resolution is the interacting force between a tip and sample.

In case of tuning fork, its high stiffness could make it difficult to get a true atomic resolution. On the contrary, Giessibl showed that the tuning fork based AFM is one of the most optimized tools to achieve the atomic resolution.[20,32] The Si 7×7 structure was imaged with excellent quality using a tuning fork as shown in Fig. 7(b). Allegedly, the detailed structure shows the chemical bonding strength between the Si adatoms. The experiment was performed in a vacuum chamber (UHV) which was designed for a commercial STM. The sample was a piece of a silicon wafer heat-treated.

In summary, the less stiff cantilever generally provides a more realistic topographic images due to weak interaction between the sample and tip, in case of

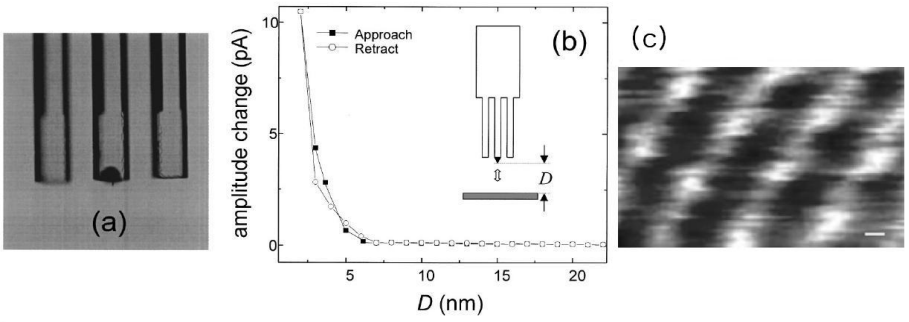

Fig. 8. (a) Optical microscope image of the trident QCR with a tip attached at the center prong. (b) A typical approach curve as a function of distance obtained in air. (c) Atomic resolution image of a mica cleaved surface. The scale bar is 1 Å. (From Seo *et al.* (2003).)

contact mode. On the contrary, in non-contact mode, the high stiffness of the tuning fork is advantageous because the interacting force can be reduced by minimizing the vibration amplitude of the tuning fork and its small thermal noise enhances the resolution. Giessibl pointed out that the vibration amplitude of the tuning fork could be reduced to about 7 Å due to its high stiffness and its small oscillation amplitude.[20]

4.3. *Trident QCR based AFM*

As Giessibl[20] proved, a QCR with a higher value of stiffness may be of much use for high resolution non-contact AFM. For instance, 1 MHz trident-type quartz tuning fork has about 100 times higher stiffness of 10^5 N/m, compared with the commonly used 32-kHz tuning fork. The high frequency of such a tuning fork is also useful in enhancing the scanning speed of scanning probe microscopes.[26] Seo *et al.* demonstrated the atomic resolution non-contact AFM by using a trident-type tuning fork as a force sensor in ambient condition.[19]

A prong of the tuning fork has the dimensions of 1.25 mm long, 93 μm thick, and 93 μm wide and its spring constant was extremely high ($k \simeq 5.4 \times 10^5$ N/m). For a trident tuning fork with $Q = 7000$, a driving voltage of 5 mV induces a current of about 100 pA corresponding to $\Delta l = 0.6$ pm. A micro-fabricated SiN cantilever tip with a 10 nm radius is manually attached, to the center prong of the trident tuning fork as shown in Fig. 8(a).

The vibration amplitude of the probe was measured as a function of the distance between the tip and sample, as shown in Fig. 8(b). The sample surface is a fleshly cleaved mica. Within a tightly sealed metal case, the humidity was reduced by placing porous silica gel. In typical operation condition, as the tip approaches and retracts, very sharp decrease and increase of the oscillation amplitude were observed without any hysteresis within 1 or 2 nm.

Figure 8(c) presents the atomic resolution image of the mica in ambient condition. This AFM image reflects the sample topography in non-contact mode. The

measured atomic corrugation was about 0.5 Å, for which the vibration amplitude was 0.6 pm and the scanned area was 1.5×1 nm^2.

5. High Sensitivity SPM

5.1. *Fine force detection method*

Generally, the magnetic or electrostatic forces ($\sim$ pN) between a tip and sample are much weaker than the repulsive atomic force ($\sim$ nN). While the atomic force is very short range, the magnetic or electrostatic forces are long range ($\geq$ 10 nm). This is a reason why the AFM has much higher spatial resolution and contrast than those of the MFM/EFM. In order to detect MFM/EFM signal, one needs a spacial technique to avoid the strong background topographic contrast, so-called *lift-mode*. In lift-mode, one scans the surface and then lifts the tip with a certain gap ($\sim$ 10 nm) and scans it again. For the tuning fork based MFM/EFM, the lift-mode is utilized, also.

There are two different force detection methods (static and dynamic) for cantilever based MFM/EFM. In static mode, a cantilever scans the sample with lift-mode and the deflection of the cantilever is measured. For dynamic mode, the resonance frequency shift is measured by using the resonance of the cantilever. In general, the dynamic mode is much sensitive than the static mode. In case of the tuning fork based MFM/EFM, the static mode is unapplicable, because it is too stiff to be deflected by the magnetic/electric force. Only using its exceptionally high Q-valued resonance, its frequency shift can be measured with the dynamic mode.

An attractive (van der Waals) force between the tip and sample can be measured by conventional cantilever based AFM, as well as repulsive force. However, its detection with a tuning fork was not easy. King *et al.* first detected the attractive force using a high Q-valued tuning fork.[33] They mounted a very tiny tip on a prong of the tuning fork, minimizing the Q-value drop. Their detection was a starting point for the attempt to improve the sensitivity of the tuning fork SPM.

5.2. *Tuning fork based MFM*

While the resonance frequency f of a tuning fork is similar to that of the cantilever, the quality factor Q and the spring constant k of a tuning fork are typically 10^2 and 10^4 times larger than those of a cantilever, respectively. Because the sensitivity of MFM is proportional to $\sqrt{Qf/k}$ with respect to the thermal noise, the tuning fork based MFM is less sensitive than the cantilever based MFM by a factor of 10.[34] This was the most serious problem of the tuning fork based MFM.

For the first time, Edwards *et al.*[24] demonstrated a tuning fork based MFM with a Fe tip. They scanned a piece of a magnetic tape and got a blurred image of the recorded magnetic pattern. Todorovic and Schultz[34] employed an etched nickel wire as a tip in a similar geometry. They used a miniature tuning fork having a stiffness k of 2000 N/m and they obtained MFM images of magnetic samples. Even

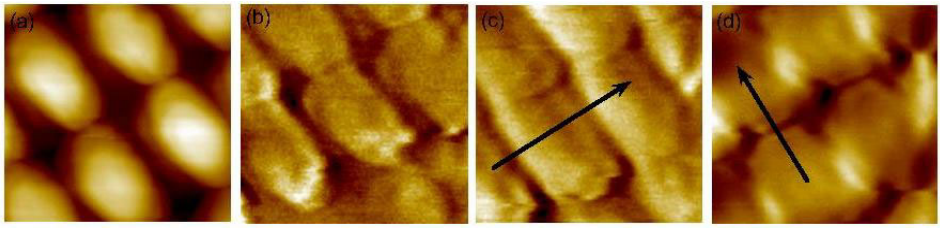

(a) (b) (c) (d)

Fig. 9. 1 μm $\times$ 1 μm simultaneous topographic (a) and MFM (b) images of an array of elliptical permalloy dots at 4.2 K, with no magnetic field. (c), (d) MFM images of the same sample at 4.2 K with an applied field of 2.5 kG. The magnetic field was applied in the direction shown by the arrows in the figures. (From Seo *et al.* (2005).)

though those groups[24,34] achieved reasonable spatial resolution (order of 100 nm), the image contrast was not satisfactory compared with that obtained by cantilever based MFM. After their publications, there have been many attempts to utilize the tuning fork as MFM sensor, especially for low temperature measurement.[35,36]

Recently, Seo *et al.* reported on high resolution (15 nm) and high sensitivity (2 pN) MFM images using a tuning fork based MFM.[37] The increased resolution and sensitivity were due to the use of tuning forks with smaller spring constants, operation at low temperatures which increased the Q of the tuning fork and improved the stability of the instrument.

Each prong of the tuning fork they used was 2.2 mm long, 190 μm thick and 100 μm wide. This geometry of the tuning fork corresponds to a value of the spring constant $k \simeq 1300$ N/m. To attach the tip, a home-made micro-manipulator with optical microscope was used. After the tip was mounted on the tuning fork, the resonance frequency decrease Δf was about 20 Hz. According to the mass loading effect of the quartz crystal microbalance technique,[38] the added mass was estimated as 0.1 μg. The resonance frequency shift and phase shift were measured by commercial PLL electronics (easyPLL from Nanosurf). They did not use any low temperature preamplifier. The tuning fork signal was passed through a coaxial cable 1 m long and was fed into a current-voltage amplifier located outside the inset. The typical dithering amplitude was 5 nm at a drive voltage of 3.5 mV at 4.2 K.

A permalloy (NiFe) sample consisting of an array of elliptical particles was imaged at 4.2 K with the external field applied in the plane of the permalloy film. The topographic image of the sample is shown in Fig. 9(a). The scanned area was 1×1 μm^2 and the excitation voltage was 7 mV. Figure 9(b) shows the MFM image of the same region without magnetic field. Judging from the contrast in each particle, it appears that each particle has its magnetization aligned along its long axis. One of many advantages of the tuning fork is compatibility for high magnetic field measurement. A magnetic field ($H = 2.5$ kG) was applied in the same condition and dramatic changes were found. Figures 9(c) and 9(d) show the resulting MFM images with the direction of magnetic field denoted by the arrows. Both images have

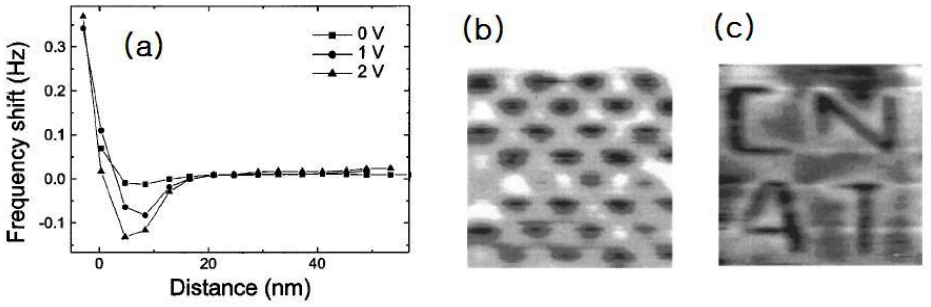

Fig. 10. (a) Approach curves obtained at bias voltages of 0, 1, and 2 V between the tip and the sample. (b)–(c) Some patterns were written on the PZT film sample. Its scanning areas were 4×4 and 7×7 μm^2, respectively. (From Seo *et al.* (2002).)

stripe patterns running at right angles to the magnetization. This was attributed to the attractive and repulsive interactions between the tip and dots, depending on their relative location.

5.3. *Tuning fork based EFM*

Seo and Jhe demonstrated the capability of the tuning fork to be utilized as an EFM sensor, first.[39] They used 1300 N/m stiffness tuning fork with $Q = 3000$ in air. A Ni tip was attached at the end of a tuning fork prong with conducting glue. Through the conducting glue, a bias voltage was applied with a small amplitude AC voltage to vibrate the fork.

Figure 10(a) shows the frequency shift as a function of distance between the tip and metallic sample. The tip was biased with DC voltages 0, 1, and 2 V, and the sample was grounded. The sharp increases of the frequency as it became close to the sample were due to the atomic force (repulsive). On the other hands, slight dips imply an attractive force. Judging from the depth change depending on bias voltages, the attractive forces are electrostatic forces induced by the charged tip. The frequency shift due the ferroelectric polarization is given by[39]

$$f \simeq \frac{1}{4}\frac{f}{k}\frac{\sigma V_{\rm dc}}{\epsilon_0}\frac{\partial C}{\partial z}\,. \tag{14}$$

A check pattern in Fig. 10(b) was written by applying $V_{\rm dc} = 10$ V (dark) and -10 V (bright), alternately. Some characters were also recorded with $V_{\rm dc} = -10$ V and read out with $V_{\rm dc} = 2$ V [Fig. 10(c)]. Note that with 300 nm width, all letters are fully resolved.

On the other hand, Wang *et al.* reported the tuning fork based EFM, also.[40] They attached a tiny tungsten tip to a tuning fork ($k = 2000$ N/m). By operating an AC modulation bias on the tip of the tuning fork, a dynamic non-contact mode electrostatic force microscope with high spatial resolution was achieved. For the

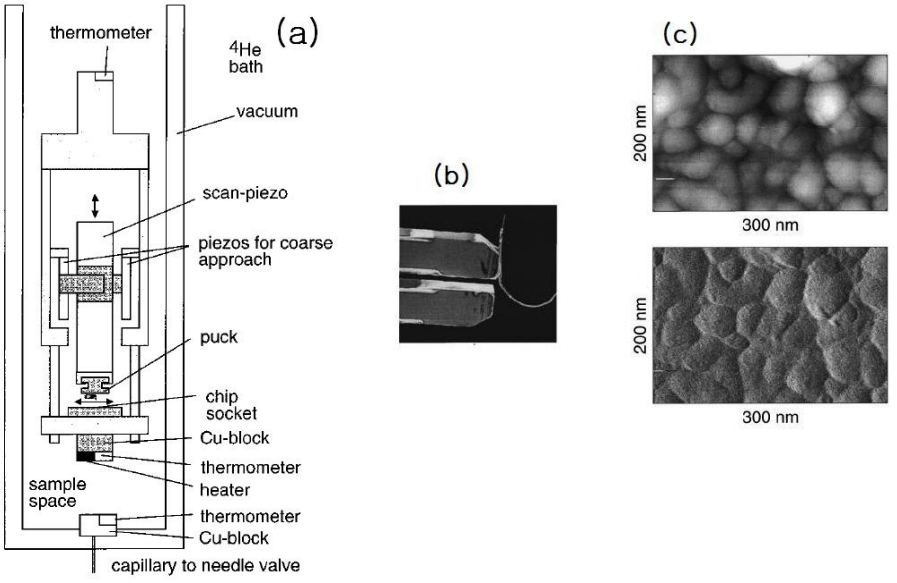

Fig. 11. (a) Schematic diagram of the low temperature SPM using a tuning fork. (b) A scanning electron micrograph of a tuning fork with a tungsten wire. (c) Surface of an evaporated gold film with 30 nm size grains was imaged at $T = 2.5$ K. Topography (top) and frequency shift (bottom) were measured, simultaneously. (From Rychen *et al.* (1999).)

topographic imaging, the van der Waals force was utilized as a feedback signal. The electrostatic force signals between the tip and the sample were measured to image quantitative surface charge density of an open-gate FET sample.

Naitou *et al.* developed a tuning fork based SCM with a remarkable spatial resolution.[41] Their PLL detection technique allowed high spatial resolution, sensitivity, and stability. The electrochemically etched W tip was attached to a prong of a quartz tuning fork ($k = 8000$ N/m). The SCM yielded two images of $\partial C/\partial V$ and $\partial C/\partial z$, where C is capacitance between the tip and sample, V a bias voltage, and z the tip-sample distance. On a cross section of a field effect transistor, the two-dimensional p-n junction was imaged with a spatial resolution better than 5 nm in the $\partial C/\partial V$ image.

6. Low Temperature SPM

The most important usage of the QCR based SPM is low temperature operation. Even though many low temperature SPM techniques have been developed, most of them have troubles to be utilized at ultra low (millikelvin) temperature, such as self-heating or large heat load due to its complicated structures. Rychen *et al.* demonstrated the low temperature capability of the tuning fork based SPM.[42] A schematic design of the low temperature SPM using a tuning fork is shown in Fig. 11(a). For the coarse approach, a slip-stick (inertial) drive was used. A puck

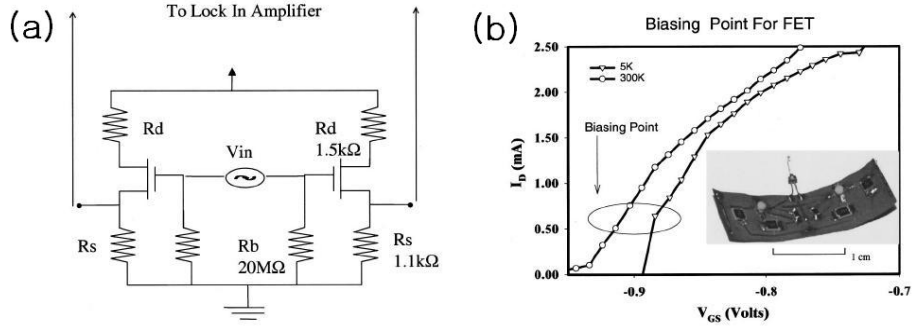

Fig. 12. (a) The circuit diagram of the preamplifier for low temperature tuning fork signal pickup. (b) The drain current (I_D) as a function of gate voltage (V_{GS}) of an epitaxial GaAs low-noise heterojunction FET. The inset shows a photograph of the preamplifier and the tuning fork. (From Patil and Levy (2002).)

mounted at the end of the tube scanner can be laterally positioned in slip-stick style, also. Figure 11(b) shows a scanning electron micrograph of a tuning fork ($k = 2000$ N/m) with a 13 mm W wire glued to the end of one prong. After the tip was mounted, the resonance frequency of the tuning fork was shifted down to 100 Hz. The Q-value was about 2×10^4 in vacuum. Figure 11(c) shows the topography and error image of a 150 nm gold film evaporated onto a glass substrate. It shows very detailed structure of grains of 30 nm size at $T = 2.5$ K.

Because the induced signal from a tuning fork has large impedance, a transimpedance amplifier is required for low temperature experiment to pick up its signal. At cryogenic temperature the large capacitive load of the long cables causes large current signal loss. To improve the signal to noise ratio, it is desirable to place a preamplifier close to the tuning fork. Patil and Levy,[43] suggested a low temperature preamplifier for tuning fork system. The preamplifier consisted of a pair of epitaxial GaAs low-noise heterojunction field effect transistors (FET).

The schematic circuit diagram of the preamplifier is shown in Fig. 12(a). Each FET was self-biased by two metal film chip resistors with 1% tolerance. This configuration allowed stable operation in the saturation region with very high input impedance. Figure 12(b) shows the drain current (I_D) as a function of gate voltage (V_{GS}) of the FET (EPB018A5-70, Excelics Semiconductors) at 300 and 4 K. The oval indicates the range of operating bias of the FET. Because it has linearity at 4 to 300 K, the preamplifier can be used without modification over the entire temperature range. It is noticeable that the circuit is designed to fit into the 1 cm diameter tip holder to locate the preamplifier close to the tuning fork as shown in the inset. The amplified signal was transmitted using a standard 50 Ω coaxial cable to a second amplifier.

Kramer *et al.* presented a NSOM designed for near-field imaging and spectroscopy at cryogenic temperature as shown in Fig. 13.[44] They successfully obtained

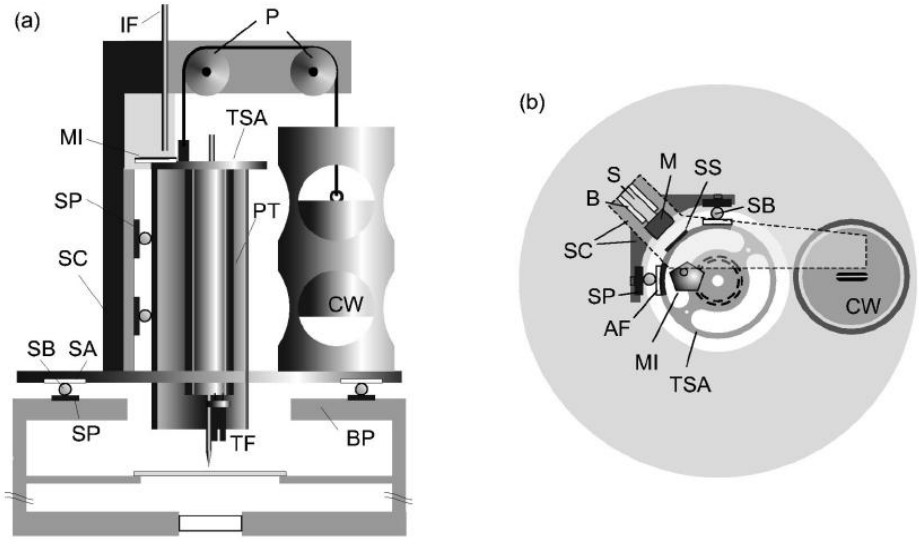

Fig. 13. Schemes of the scan head in side view (a) and top view (b): tube scanner assembly (TSA), piezo tube (PT), tuning fork (TF), static counterpart (SC), base plate (BP), shear piezo stack (SP), sapphire ball (SB), sapphire plate (SA), interferometer fiber (IF), mirror (MI), pulley (P), counter weight (CW), bearing (B), screw (S), magnet (M), steel sheet (SS), aluminum plane face (AF). (From Kramer *et al.* (2002).)

topographic images of a silicon grating sample, on immersion into superfluid helium ($T = 1.8$ K). For a z-directional coarse approach mechanism, two shear piezo stacks were employed with a slip-stick motion. A counter weight was used to compensate the downward gravity due to the weight of the head part in coarse approach mechanism. They found an amplitude fluctuation related with the superfluidity of the helium. Nevertheless, a stable distance feedback was achieved when the set value of the frequency shift was chosen slightly larger than the fluctuation amplitude.

Recently, Brown *et al.* developed a millikelvin temperature range (100 mK) SPM with a tuning fork.[45] They used a W tip glued on the tuning fork and a PLL (EasyPLL, Nanosurf) detection scheme with 5 mHz sensitivity. Their preamplifier was based upon a low-noise Si junction field effect transistor (JFET) that did not work below 60 K. The other components of the preamplifier operated at 4.2 K. Therefore, they designed the preamplifier allowing the JFET to heat above 60 K and the other parts to be anchored at 4.2 K stage.

7. Conclusion

The QCR including tuning fork is a useful force sensor for almost all kinds of SPMs. The advantages of the QCR based SPM compared with a conventional cantilever based SPM are non-optical detection, small vibration amplitude, self-actuating and

self-sensing, low power dissipation, etc. Especially, for low temperature experiments exploring nano-scale nature, tuning fork base SPM is very promising tool, because of its low power dissipation, simple design, and high spatial resolution.

Acknowledgments

This work was supported by the Post-doctoral Fellowship Program of Korea Science and Engineering Foundation (KOSEF).

References

1. G. Binnig, H. Rohrer, Ch. Gerber and E. Weibel, *Phys. Rev. Lett.* **49** (1982) 57.
2. G. Binnig, C. F. Quate and Ch. Gerber, *Phys. Rev. Lett.* **56** (1986) 930.
3. D. W. Pohl, W. Denk and M. Lanz, *Appl. Phys. Lett.* **44** (1984) 651.
4. Y. Martin and H. K. Wickramasinghe, *Appl. Phys. Lett.* **50** (1987) 1455.
5. J. J. Saenz, N. Garcia, P. Grütter, E. Meyer, H. Heinzelmann, R. Wiesendanger, L. Rosenthaler, H. R. Hidber and H.-J. Güntherodt, *J. Appl. Phys.* **62** (1987) 4293.
6. Y. Martin, D. W. Abraham and H. K. Wickramasinghe, *Appl. Phys. Lett.* **52** (1988) 1103.
7. A. Moser, H. J. Hug, I. Parashikov, B. Stiefel, O. Fritz, H. Thomas, A. Baratoff, H.-J. Güntherodt and P. Chaudhari, *Phys. Rev. Lett.* **74** (1995) 1847.
8. W. Allers, A. Schwarz, U. D. Schwarz and R. Wiesendanger, *Rev. Sci. Instrum.* **69** (1998) 221.
9. C. W. Yuan, E. Batalla, M. Zacher, A. L. de Lozanne, M. D. Kirk and M. Tortonese, *Appl. Phys. Lett.* **65** (1994) 1308.
10. A. Volodin, K. Temst, C. Van Haesendonck and Y. Bruynseraede, *Rev. Sci. Instrum.* **71** (2000) 4468.
11. V. E. Bottom, *Introduction to Quartz Crystal Unit Design* (Van Nostrand Reinhold Company, 1982), p. 62.
12. F. J. Giessibl, *Appl. Phys. Lett.* **73** (1998) 3956.
13. T. Ono, Y. Lin and M. Esashi, *Appl. Phys. Lett.* **87** (2005) 074102.
14. W. Clauss, J. Zhang, D. J. Bergeron and A. T. Johnson, *J. Vac. Sci. Technol.* **17** (1999) 1309.
15. Z. Peng and P. West, *Appl. Phys. Lett.* **86** (2005) 014107-1.
16. J. B. Marion, *Classical Dynamics of Particles and Systems* (Univ. Maryland, College Park, 1995).
17. D. Sarid, *Scanning Force Microscopy*, Chap. 1 (Oxford University Press, New York, 1991).
18. K. Karrai and R. D. Grober, *Appl. Phys. Lett.* **66** (1995) 1842.
19. Y. Seo, H. Choe and W. Jhe, *Appl. Phys. Lett.* **83** (2003) 1860.
20. F. J. Giessibl, *Appl. Phys. Lett.* **76** (2000) 1470.
21. R. D. Grober, J. Acimovic, J. Schuck, D. Hessman, P. J. Kindlemann, J. Hespanha, A. S. Morse, K. Karrai, I. Tiemann and S. Manus, *Rev. Sci. Instrum.* **71** (2000) 2776.
22. P. Guethner, U. Fischer and K. Dransfeld, *Appl. Phys. B: Photophys. Laser Chem. B* **48** (1989) 89.
23. W. A. Atia and C. C. Davis, *Appl. Phys. Lett.* **70** (1997) 405.
24. H. Edwards, L. Taylor, W. Duncan and A. J. Melmed, *J. Appl. Phys.* **82** (1997) 980.
25. D. P. Tsai and Y. Y. Lu, *Appl. Phys. Lett.* **73** (1998) 2724.
26. Y. Seo, J. H. Park, J. B. Moon and W. Jhe, *Appl. Phys. Lett.* **77** (2000) 4274.
27. Y. Seo and W. Jhe, *Rev. Sci. Instrum.* **73** (2002) 2057.

28. Y. D. Wilde, F. Formanek and L. Aigouy, *Rev. Sci. Instrum.* **74** (2003) 3889.
29. S. Kim, H. Yoo, K. Lee, B. Friedman, M. A. Gaspar and R. Levicky, *Appl. Phys. Lett.* **86** (2005) 153506.
30. W. H. J. Rensen, N. F. van Hulst and S. B. Kämmer, *Appl. Phys. Lett.* **77** (2000) 1557.
31. M. Koopman, B. I. de Bakker, M. F. Garcia-Parajo and N. F. van Hulst, *Appl. Phys. Lett.* **83** (2003) 5083.
32. F. J. Giessibl, S. Hembacher, H. Bielefeldt and J. Mannhart, *Science* **289** (2000) 422.
33. G. M. King, J. S. Lamb and G. Nunes, Jr., *Appl. Phys. Lett.* **79** (2001) 1712.
34. M. Todorovic and S. Schultz, *J. Appl. Phys.* **83** (1998) 6229.
35. S. Rozhok and V. Chandrasekhar, *Solid State Commun.* **121** (2002) 683.
36. S. Rozhok, S. Jung, V. Chandrasekhar, X. Lin and V. P. Dravid, *J. Vac. Sci. Technol. B* **21** (2003) 323.
37. Y. Seo, P. Cadden-Zimansky and V. Chandrasekhar, *Appl. Phys. Lett.* **87** (2005) 103103.
38. C. D. Stockbridge, *Vac. Microbalance Tech.* **5** (1966) 147.
39. Y. Seo and W. Jhe, *Appl. Phys. Lett.* **80** (2002) 4324.
40. Z. Wang, J. Bao, H. Zhang and W. Guo, *Appl. Phys. Lett.* **81** (2002) 1300.
41. Y. Naitou and N. Ookubo, *Appl. Phys. Lett.* **83** (2004) 2131.
42. J. Rychen, T. Ihn, P. Studerus, A. Herrmann and K. Ensslin, *Rev. Sci. Instrum.* **70** (1999) 2765.
43. N. G. Patil and J. Levy, *Rev. Sci. Instrum.* **73** (2002) 486.
44. A. Kramer, J.-M. Segura, A. Hunkeler, A. Renn and B. Hecht, *Rev. Sci. Instrum.* **73** (2002) 2937.
45. K. R. Brown, L. Sun and B. E. Kane, *Rev. Sci. Instrum.* **75** (2002) 2029.